Original Article

Institution of MECHANICAL ENGINEERS
Journal of POWER AND ENERGY

Proc IMechE Part A:
J Power and Energy
2014, Vol. 228(3) 340–356

DOI: 10.1177/0957650913517677
pia.sagepub.com
SAGE

Selection and thermodynamic analysis of a turbocharger for a producer gas-fuelled multi-cylinder engine

Anand M Shivapuji and S Dasappa

Abstract

The current work addresses the use of producer gas, a bio-derived gaseous alternative fuel, in engines designed for natural gas, derived from diesel engine frames. Impact of the use of producer gas on the general engine performance with specific focus on turbo-charging is addressed. The operation of a particular engine frame with diesel, natural gas and producer gas indicates that the peak load achieved is highest with diesel fuel (in compression ignition mode) followed by natural gas and producer gas (both in spark ignite mode). Detailed analysis of the engine power de-rating on fuelling with natural gas and producer gas indicates that the change in compression ratio (migration from compression to spark ignited mode), difference in mixture calorific value and turbocharger mismatch are the primary contributing factors. The largest de-rating occurs due to turbocharger mismatch. Turbocharger selection and optimization is identified as the strategy to recover the non-thermodynamic power loss, identified as the recovery potential (the loss due to mixture calorific value and turbocharger mismatch) on operating the engine with a fuel different from the base fuel. A turbocharged after-cooled six cylinder, 5.9 l, 90 kWe (diesel rating) engine (12.2 bar BMEP) is available commercially as a naturally aspirated natural gas engine delivering a peak load of 44.0 kWe (6.0 bar BMEP). The engine delivers a load of 27.3 kWe with producer gas under naturally aspirated mode. On charge boosting the engine with a turbocharger similar in configuration to the diesel engine turbocharger, the peak load delivered with producer gas is 36 kWe (4.8 bar BMEP) indicating a de-rating of about 60% over the baseline diesel mode. Estimation of knock limited peak load for producer gas-fuelled operation on the engine frame using a Wiebe function-based zero-dimensional code indicates a knock limited peak load of 76 kWe, indicating the potential to recover about 40 kWe. As a part of the recovery strategy, optimizing the ignition timing for maximum brake torque based on both spark sweep tests and established combustion descriptors and engine-turbocharger matching for producer gas-fuelled operation resulted in a knock limited peak load of 72.8 kWe (9.9 bar BMEP) at a compressor pressure ratio of 2.30. The de-rating of about 17.0 kWe compared to diesel rating is attributed to the reduction in compression ratio. With load recovery, the specific biomass consumption reduces from 1.2 kg/kWh to 1.0 kg/kWh, an improvement of over 16% while the engine thermal efficiency increases from 28% to 32%. The thermodynamic analysis of the compressor and the turbine indicates an isentropic efficiency of 74.5% and 73%, respectively.

Keywords

Alternative fuels, producer gas, gas engines, de-rating, turbo-charging

Date received: 25 May 2013; accepted: 18 November 2013

Introduction

Bio-derived alternative fuels are gaining prominence in the energy sector[1] owing to their potential to address, albeit partially, the economic[2] and environmental challenges[3,4] brought about by the unrestrained use of conventional fuels. While alternative fuels are gaining prominence and their adoption becoming imperative, the rather significant differences in the thermo-physical properties of these fuels[5–8] compared to conventional hydrocarbon fuels pose a fundamental challenge in fuelling energy conversion devices, especially internal combustion (IC) engines. This is compounded further by the limited availability of dedicated engines for bio-derived alternative fuels,[9] forcing the unmodified use of engines designed for conventional fuels. Fuelling of unmodified conventional fuel engines with alternative fuels introduces power de-rating[10] as one of the primary penalties. Engine de-rating leads to higher cost per kWh for

Center for Sustainable Technologies, Indian Institute of Science, Bangalore, India

Corresponding author:
Anand M Shivapuji, Center for Sustainable Technologies, Indian Institute of Science, Bangalore 560012, India.
Email: anandms@cgpl.iisc.ernet.in

the energy produced[11,12] and an increase in the capital cost per kW rating,[13,14] adversely affecting the economics of power generation.[15] Resolving the described challenge requires a detailed analysis of the factors contributing to the engine de-rating which can then be used to evolve power recovery strategies.

The current work addresses the power de-rating issues associated with the operation of engines designed for natural gas (NG) derived from diesel engine frames on fuelling with producer gas (PG), a low calorific value (LCV) bio-derived gaseous alternative fuel. A detailed analysis of the various contributing factors points to the under-performance of turbochargers with PG-fuelled operation as one of the critical factors, suggesting the need for turbocharger optimization. The details pertaining to the identification and quantification of factors contributing to power de-rating and the basis for turbocharger selection and optimization as the power recovery strategy are discussed in the following sections.

Quantifying de-rating contributing factors

Towards identifying and quantifying the various factors contributing to engine de-rating, the performance of three engines of Cummins India Limited (CIL) with different power rating and displacement volume capacity is compared when operated with diesel, NG and PG. Each of the three engines is baseline diesel engines suitably adopted for NG and PG operation. The engines are identified as E-500, E-250 and E-90, respectively, with the numbers 500, 250 and 90 referring to the nominal diesel rating in kW. The diesel and NG data are from CIL specifications while the data for PG-fuelled turbocharged after-cooled (TA) operation have been reported by Dasappa et al.[9,10] The detailed engine specifications and performance with the three fuels are tabulated in Tables 9–11 in the Appendix 2. The critical results are consolidated and presented as a bar chart in Figure 1.

De-rating due to compression ratio reduction. In the adoption of a diesel engine for gas operation, reduction of compression ratio (CR) is mandatory to prevent engine knock.[11] A simple thermodynamic analysis indicates that a reduction in the CR leads to engine power de-rating. While the change in the Otto cycle efficiency is under 1% per unit change of CR for higher CR values ($CR > 14$), it is in close to 2% for lower CR values ($CR < 9$). This has been verified by Dasappa[16] in comparing the performance of various gas engines derived from diesel frames. On the basis of comparisons, Dasappa has established that a unit change in CR can change the engine peak power rating between 1% and 3% from the nominal output. With a CR reduction of 3.1, 5.5 and 6.0 units on the engines E-500, E-250 and E-90, respectively, and considering a power reduction of 3% per unit CR reduction, the engines experience a thermodynamic de-rating of 46.5 kWe, 41.2 kWe and 16.2 kWe, respectively, as indicated in Figure 1.

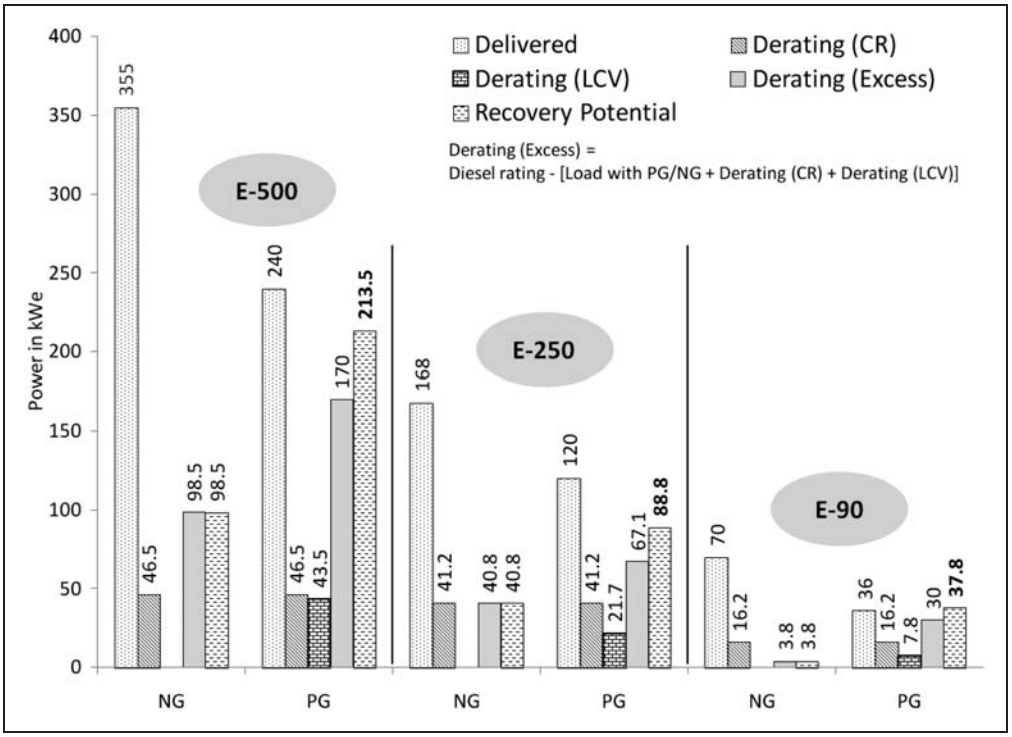

Figure 1. Power de-rating distribution comparison for the three engines.
LCV: low calorific value; CR: compression ratio; NG: natural gas; PG: producer gas.

De-rating due to thermo-physical properties of the fuel. Producer gas, generated from the thermochemical conversion of biomass in an open top dual air entry down-draft gasifier (IISc design)[17] typically contains $19 \pm 1\%$ of H_2, $19 \pm 1\%$ of CO, $1.8 \pm 0.4\%$ CH_4, $9.0 \pm 1\%$ CO_2 and balance N_2 on dry basis and has an LCV of about 5.0 MJ/kg. The thermo-physical properties of PG,[18,19] which are significantly different from conventional fuels, are presented in Table 1 and are compared with the properties of gasoline, H_2 and CH_4.[11,20,21] Preliminary analysis suggests power de-rating of an engine designed for conventional fuels when operated with PG due to the low stoichiometric mixture LCV, adiabatic flame temperature and lower than unity product to reactant mole ratio.[16,22,23] The de-rating due to the lower mixture LCV of PG in comparison with diesel (considering lean but close to stoichiometric operation at rated load) evaluates to 43.5 kWe, 21.7 kWe and 7. kWe for the engines E-500, E-250 and E-90, respectively, as indicated in Figure 1.

Load imbalance and additional de-rating factor. Theoretically, the load delivered by the substitute fuel along with the quantified de-rating factors should add up to the nominal diesel rating within a small % of error. Attempting such a balance for the three engines, however, indicates that a substantial unbalanced de-rating component exists which is the highest of all the de-rating components. The additional de-rating for NG and PG operation is 98.5 kWe and 170 kWe on E-500, 40.8 kWe and 67.1 kWe on E-250 and 3.8 kWe and 30 kWe on E-90, respectively. Having identified and quantified the other de-rating factors, the only plausible reason for this additional de-rating stems from a potential constraint on the mass of the mixture supplied to the engines. This is verified from the gas mass flow measurements on each engine. The constraint on the gas mass flow is traced to the low pressure ratio achieved across the compressor of the turbocharger on each of the engines. The pressure ratio is 1.5 for the engines E-500 and E-250 and 1.2 for E-90 opposed to 2.4 under corresponding diesel mode. Thus, the additional de-rating is attributed to the inability of the turbocharger to provide the required quantity of fuel-air mixture to the engine, indicating engine-turbocharger mismatch under the new operating conditions.

Diesel engines being quality governed with unthrottled air supply, maintain nearly constant and high exhaust flow rates over the entire load range and accordingly have large sized turbochargers. In adapting from compression ignition (CI) to spark ignited (SI) operation, the engine changes to quantity governed throttled operation, and the turbocharger turbine receives low enthalpy exhaust at low mass flow rates especially in the low and no load condition(s). This leads to turbocharger lag, which subsequently limits the attainable pressure ratio and the peak engine load, indicating engine-turbocharger mismatch.

Power recovery strategy: Turbocharger selection

Among the three factors contributing to engine power de-rating, the de-rating due to CR reduction represents a thermodynamic constraint while the other two factors are non-thermodynamic in nature with a potential for recovery. The power de-rating due to turbocharger mismatch and low mixture LCV is accordingly designated as the power recovery potential (refer Figure 1). The total recovery potential for PG operation is estimated at 213.5 kWe, 88.8 kWe and 37.8 kWe on the engines E-500, E-250 and E-90, respectively. The recovery can be realized by increasing the mass flow to the engine which is in turn possible by turbocharger selection and optimization to suit the mass flow requirements to achieve the desired power output. Thus, turbocharger selection is adopted as the strategy for power recovery.

Peak load projection using zero-dimensional code

Having estimated the recovery potential and the corresponding peak load, it would be very useful to assess the peak load capacity of the engine frame on the new fuel by using engine simulation tools. Towards this end, a zero-dimensional Wiebe function-based[24] model with knock prediction capabilities, developed in-house, was used for engine simulation. The zero-dimensional model predicts a knock limited

Table 1. Comparison of thermophysical properties of PG with convention fuels.

	Gasoline	H_2	CH_4	PG
Air-fuel ratio (kg/kg) at $\phi = 1$	14.7	34.3	17.0	1.30
Fuel lower calorific value (MJ/kg)	44.4	121	50.2	5.00
Mixture calorific value (MJ/kg) at $\phi = 1$	2.82	3.42	2.78	2.17
Product to reactant mole ratio at $\phi = 1$	1.05	0.85	1.00	0.90
Flame speed (m/s) at $\phi = 1$	0.41	2.37	0.42	0.50
Adiabatic flame temperature (K) at $\phi = 1$	2580	2480	2214	1873

PG: producer gas.

load of 76 kWe at average manifold pressure of 1.85 bar and is significantly close to the estimated peak load of 74 kWe. Details regarding the model development and simulation results are presented in subsequent sections.

Need for and scope of the current intervention

The criticality of turbocharger selection and optimization as a strategy for power recovery with PG-fuelled operation is evident from the above discussion(s). Literature survey indicates very limited fundamental work on PG engines, with most of the literature being primarily on the performance analysis of PG-fuelled engines.[9,10,25–27] The authors find no work that holistically analyses and quantifies the various de-rating components and suggests suitable strategy for power recovery.

The current work, seeking to bridge the gap in the literature, reports on the methodology adopted towards the selection of a turbocharger to recover the load designated as recovery potential on the engine E-90 for PG-fuelled operation. The limiting condition for engine operation is established using experimental and modelling results. Engine performance analysis based on the in-cylinder pressure trace(s) is reported along with the thermodynamic analysis of the optimized turbocharger. With the turbochargers being of fixed blade type, no attempt to geometrically optimize the turbocharger is addressed.

Materials and methods

Engine and turbocharger specifications

The specifications of the engine and turbochargers used in the present investigation are presented in Tables 2 and 3, respectively.

Instrumentation

The in-cylinder pressure is measured using an AVL make spark plug adapted, un-cooled, piezo-electric, differential pressure sensor (GH13Z) at an acquisition frequency of 90 kHz. Differential to absolute conversion is by using a manifold pressure sensor with a reference pressure supplement. Pressure measurement across the compressor and turbine is by means of a line pressure sensor with an absolute pressure supplement. Data are acquired using an eight-channel acquisition module (AVL IndiModul) while real-time processing and display is by means of a graphical user interface (AVL IndiCom).

Table 2. Specifications of the engine.

Engine make and model	Cummins India Limited – 6B5.9
Rated output (turbocharged)	90 kWe on diesel and 70 kWe on NG
Cylinders/displacement	6/5.9 l
Engine speed	1500 rpm
Compression ratio	16.5 in CI mode and 10.5 in SI mode

Methodology

While experimental investigations form the core of the present work, the zero-dimensional model provides an extremely valuable input in terms of the knock limited peak load supported by the engine. As such, a brief discussion on the model development along with the experimental investigation methodology is covered in the present section.

Zero-dimensional model development. The zero-dimensional model to predict the evolution of cylinder pressure during the cycle is developed based on the first law[11] as in equation (1). The gas exchange process and mass flow through the various volumes are modelled along the filling and emptying technique (FET)[28] and the one-dimensional compressible isentropic flow equation, respectively

$$\frac{\mathrm{d}P}{\mathrm{d}\theta} = \frac{(\gamma-1)}{V}\frac{\mathrm{d}Q}{\mathrm{d}\theta} - \gamma\frac{P}{V}\frac{\mathrm{d}V}{\mathrm{d}\theta} + \frac{(\gamma-1)}{V} \times \left[\frac{c_i^2}{(\gamma_i-1)}\frac{\mathrm{d}m_i}{\mathrm{d}\theta} - \frac{c_e^2}{(\gamma_e-1)}\frac{\mathrm{d}m_e}{\mathrm{d}\theta}\right] \quad (1)$$

The energy released in the cylinder due to combustion is modelled using the Wiebe function of the form as in equation (2) where the constant 'm' is the shape factor, while 'a' is the efficiency factor, indicative of the fuel conversion efficiency. For conventional fuels, the shape and efficiency factors have been optimized at 2 and 5, respectively. The subscripts 'soc' and 'doc' indicate the start and duration of combustion, respectively

$$\frac{Q_{chem}(\theta)}{Q_{chem-total}} = 1 - exp\left[-a\left(\frac{\theta-\theta_{soc}}{\Delta\theta}\right)^{m+1}\right] \quad (2)$$

A chemical kinetics module composed of 53 species in a reaction mechanism involving 325 reactions is developed and integrated with the Wiebe function-based module to enable knock prediction. At each crank angle, the change in the specie concentration and hence the enthalpy, pressure and temperature of the mixture is evaluated by simultaneously solving for all the specie concentration change rate equations. On attaining the necessary conditions during the course of the cycle, the end mixture corresponding to the instantaneous un-burned mass fraction auto-ignites, leading to lumped energy release and a sudden rise in the temperature and pressure.

The detailed description of the Wiebe function-based engine model development and validation has been presented by the authors in Ref. 29 while extending the model to include knock prediction has been covered in Ref. 30.

Experimental investigations. With a mandate for turbocharger selection to realize the established load, the preliminary turbocharger selection is based on the volume flow rate/power rating range of turbochargers, available as specifications. The mass flow rate (pseudo non-dimensional) and the corresponding pressure boost required for the range of loads are calculated based on the specific fuel consumption (SFC) under PG-fuelled NA mode of operation (available from previous works by the authors[9,23]) and mapped onto the compressor maps of the turbochargers short listed in the preliminary selection. Four HX series turbochargers designated as $TC-1$, $TC-2$, $TC-3$and $TC-4$ (refer Table 3) are selected for further experimental investigation. The turbocharger selection details are presented in the next section.

Each of the four turbochargers is individually mounted onto the engine, and the engine is operated to identify the peak supported load. The turbocharger that delivers the desired load is selected as the optimal turbocharger and a detailed experimental investigation is carried out to qualify the turbocharger for PG operation at the desired load.

Turbocharger selection

Preliminary turbocharger selection is based on mapping the estimated pressure ratio and the corresponding mass flow required for achieving the designated load, identified previously, onto the compressor maps. The mixture mass flow required to achieve this load is estimated based on the NA mode SFC. The pressure ratio is the ratio of the designated load mass flow rates to the NA peak load mass flow rate. This initial pressure ratio is subsequently corrected to account for the temperature rise. The details are as discussed below.

Peak load and SFC for NA mode of operation

The peak load delivered by the engine under PG-fuelled NA mode operation has been reported (refer Ref. 23 by the current authors) at 27.32 kWe with the brake specific biomass and gas consumption being 1.25 ± 0.05 kg/kWh and 3.24 kg/kWh, respectively.

Mass flow rate and pressure ratio estimation

Towards estimating the mixture mass flow rate at the designated load under TA operation, the NA mode mixture consumption was considered. While engine operation near rated load leads to an improvement in SFC,[11,31] the use of NA mode SFC would suggest higher mass flow rate and pressure ratio. This is justified considering that selection of a slightly overrated turbocharger is better than selecting an underrated turbocharger. The pressure ratio across the compressor is estimated considering the mixture density to be a function of mass and temperature. The ratio of mass flow rate at the desired load and NA peak load gives the initial pressure ratio from which the isentropic exit temperature is estimated (equation (3)). The actual exit temperature is estimated using equation (4) assuming isentropic efficiency of 75%.[9,32,10] The initial pressure ratio is corrected to account for the temperature rise by using the equation of state as in equation (5). The pseudo mass flow parameter and the corresponding pressure ratio for the 50% to 100% load range are listed in Table 4

$$\frac{T_{TA}}{T_{NA}} = \frac{P_{TA}}{P_{NA}}^{\frac{\gamma-1}{\gamma}} \tag{3}$$

$$\eta_{is-c} = \frac{T_{e-is} - T_i}{T_e - T_i} \tag{4}$$

$$\frac{P_{TA}}{P_{NA}} = \frac{\rho_{TA}}{\rho_{NA}} \frac{T_{TA}}{T_{NA}} \tag{5}$$

Table 3. Turbocharger specifications.

Make	Holset/CTT			
Designation	TC – 1	TC – 2	TC – 3	TC – 4
Volumetric capacity range (l)	5.0–6.5 at PR 3		Up to 5 at PR 3	
Peak flow rate (kg/s)	0.46		0.35	
Power range (kW)	75–208		67–179	
Turbine housing cross-sectional area ($\times 10^{-4}$ m^2)[a]	10	8	6	8
Compressor wheel diameter (mm)	82	77	68	

[a]The compressor discharge cross-sectional area to radius (A/R) is generally mentioned. Cumming Turbo Technologies (CTT) however specifies the turbine housing cross-sectional area in lieu of A/R.

Table 4. Estimated pressure ratio and pseudo non-dimensional mass flow values.

Load		Compressor pressure ratio (bar/bar)	Pseudo mass flow rate ($(kg/s).\frac{\sqrt{K}}{MPa}$)
%	kWe		
100	73.8	2.43	20.39
90	66.4	2.14	18.32
80	59.0	1.84	16.25
70	51.7	1.60	14.54
60	44.3	1.31	12.45
50	36.9	1.04	10.36

Data mapping and turbocharger selection

Among the different series available with cumming turbo technologies (CTT) (scuh as H1, H2, HE, HX, HY,...), preliminary assessment, based on the load and flow rate range (refer Table 4), suggests HX series turbochargers as being suitable for the desired load and mixture flow rate. With the mapping of the mass flow and pressure ratio data on compressor maps of the HX series turbochargers, two turbochargers qualify to be evaluated based on the position of the operating regime with respect to the surge–choke limits.[33] The compressor maps with the operating points for the existing turbocharger (optimized for diesel operation) and the two other turbochargers are as in Figure 2 (a) to (c). The turbochargers TC–3 and TC–4 have a common compressor with a provision for changing the turbine housing from 6 cm^2 (TC–3) to 8 cm^2 (TC–4) area.

Superimposing the projected operating points for PG operation on the compressor map of TC–1, (Figure 2a), it can be observed that, up to about 65% of the PG peak load, the operating points fall outside the operating range of the turbocharger and at about 85% of the PG peak load the surge line is crossed. The typical diesel operation in the 80% to 100% load range (SFC around 0.21 and A/F around 19[34–36]) is also mapped for comparison. The mismatch of turbocharger TC–1 for PG operation is evident.

Experimental results

Experimental investigations involved identifying the maximum brake torque (MBT) ignition timing for PG-fuelled operation and the peak load supported by each of the turbochargers. Once the optimal turbocharger is identified, a complete parametric investigation of turbocharged engine operation spanning no load to full load operation is carried out.

MBT ignition timing for PG-fuelled operation

On fuelling a NG engine with PG, the MBT spark timing needs to be adjusted considering that PG has thermo-physical properties significantly different from NG. Towards identifying the MBT timing with PG, spark sweep test is carried out under both NA and turbocharger mode. Figure 3 presents outcome of the spark sweep test, identifying the peak load at different crank angles, under NA and TA mode (optimized turbocharger) of operation. The MBT timing is at 24° before the top dead centre (TDC) for NA mode while it is 22° before TDC for TA mode of operation. The TA mode MBT angle is 2° advanced as compared to NA mode operation due to higher in-cylinder turbulence under TA mode than NA mode which increases the turbulent flame propagation rate. The MBT timing for PG-fuelled operation is advanced by 4° and 6°, respectively, for NA and TA mode as compared to NG operation due to significantly higher flame speed for PG as compared to NG (refer Table 1).

It is well established that the nature of combustion phasing under MBT ignition settings remains substantially similar for all operating conditions and fuels[37] and as such features inferred from the in-cylinder pressure profiles, known as combustion descriptors, have a fixed value under MBT operation. Considering that multiple turbocharger combinations had to be tested, and with the time and resource intensive nature of spark sweep tests, recourse of identifying the MBT timing by position of the combustion descriptors was adapted. The position of peak pressure has been established as one of the most versatile combustion descriptors[38] and has a value between 10° and 15° after TDC (close to 15) for MBT operation. The MBT ignition setting for PG-fuelled operation is established (also verified for NA and optimized TA operation) from the position of peak pressure as indicated in Figure 4. The angles of 24° and 22° before TDC as MBT ignition angles are evident.

Peak supported load on the engine with different turbochargers

The outcome of engine operation with different turbochargers is consolidated in Table 5. The turbocharger TC–1 and TC–2 supported a peak load of 35.0 kWe and 40.0 kWe, respectively, being limited by engine de-speeding. The testing of TC–3 had to be aborted at 25.0 kWe as the turbine inlet temperature and the exit pressure approached the limiting values specified for safe operation. The 6B5.9 engine with the TC–4 delivered a knock limited peak load of 72.8 kWe, indicating near complete recovery of the identified potential, with all the safety parameters within limits.

The peak load 250 cycle ensemble average pressure–crank angle traces for the engine with turbochargers TC–1, TC–2 and TC–4 are shown in Figure 5. The MBT operation of the engine is apparent with the peak pressure being positioned at 15° after TDC. Two traces indicating (potential) end gas auto-ignition when the engine was loaded beyond 72.8 kWe are

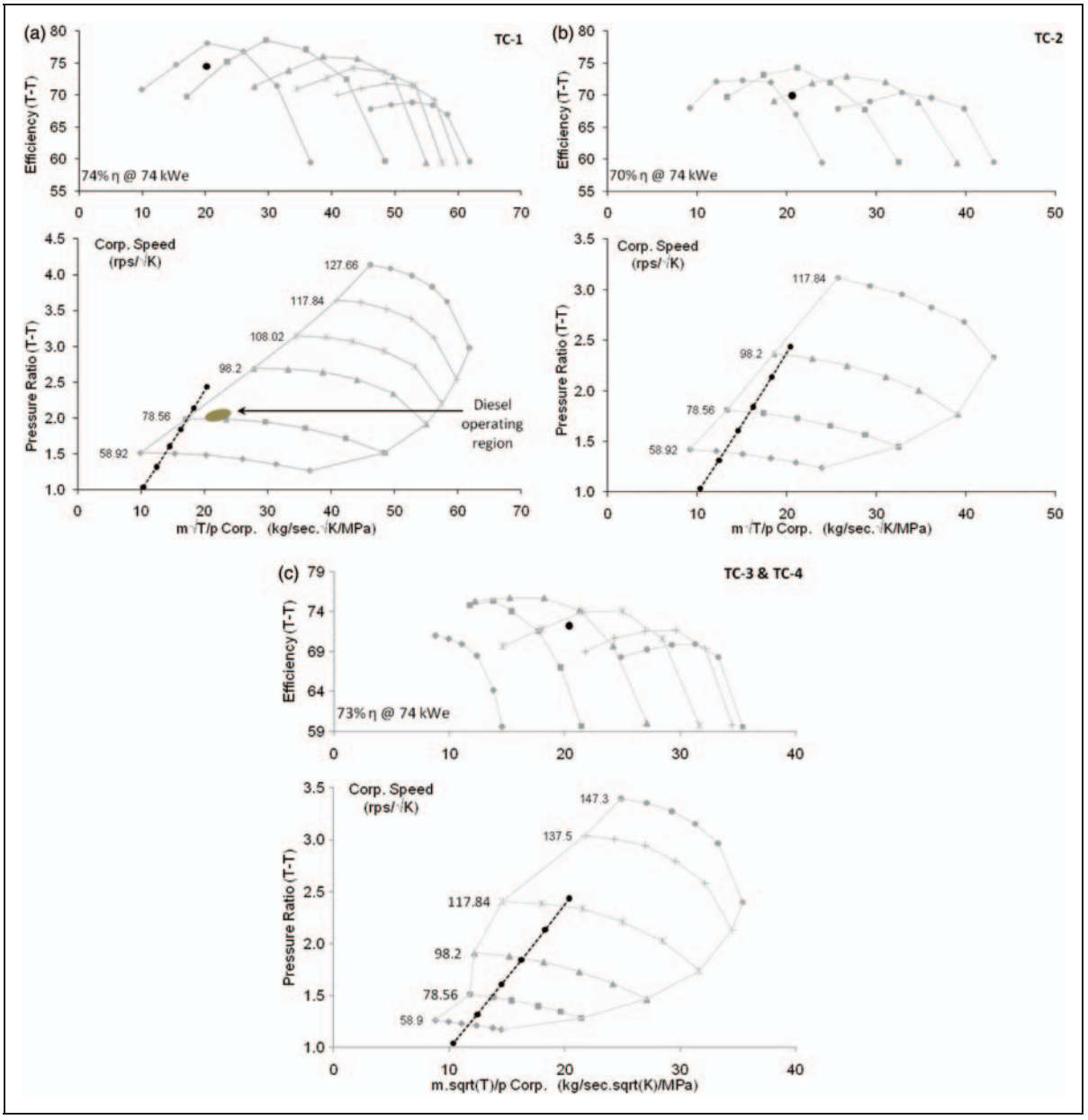

Figure 2. (a) Compressor map for TC–1. (b) Compressor map for TC–2. (c) Compressor map for TC–3 and TC–4.

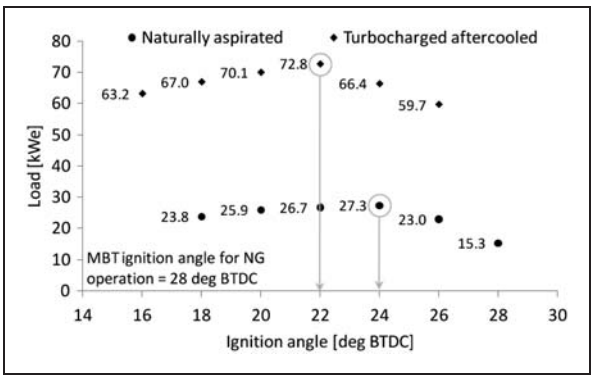

Figure 3. Spark sweep test for establishing the MBT ignition timing.
MBT: maximum brake torque; NG: natural gas; BTDC: before top dead center.

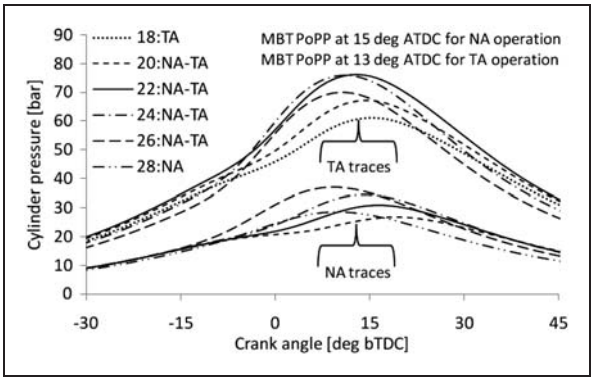

Figure 4. Pressure-crank angle traces for the spark sweep test.
MBT: maximum brake torque; ATDC: after top dead center; NA: naturally aspirated; TA: turbocharged after-cooled.

Table 5. Consolidation of turbocharger testing outcome.

Turbocharger	Load (kWe)	Remarks
TC–1	35.0	Peak supported load below the target
TC–2	40.0	Peak supported load below the target
TC–3	25.0	Testing suspended due to safety concerns
TC–4	72.8	Peak supported load, (98.4% of the target load)

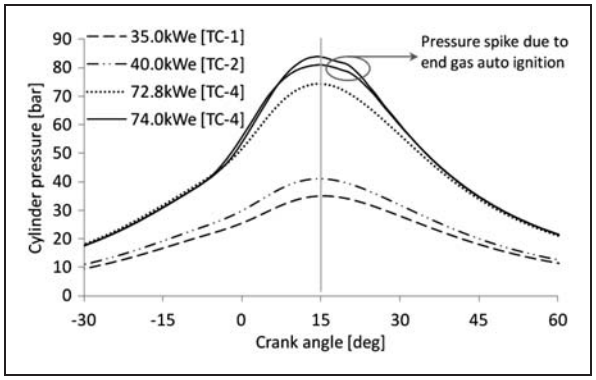

Figure 5. Peak load pressure crank angle diagram.

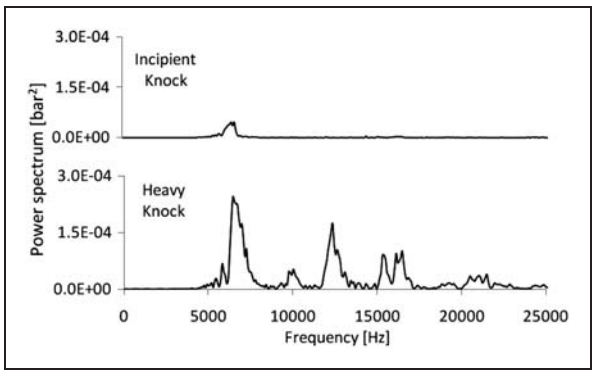

Figure 6. Spectral analysis of knocking cycles.

also shown. At 74.0 kWe, a small spike is evident in the vicinity of 20° after TDC but no high frequency oscillations are observed, indicating incipient knock.[11,39] Towards on-line identification of knock (incipient and heavy), the pressure signal is subjected to spectral analysis to identify the exciting frequencies. It has been established that knock excites characteristics frequencies in the 5 kHz to 7 kHz range and a presence of these frequencies in the spectrum indicates knock[40,41] as depicted in Figure 6.

Analysis of modelling and experimental results

The outcome of engine modelling along with the analysis of experimental data is presented in this section.

Peak load prediction by the zero-dimensional model

The zero-dimensional model requires the mixture pressure, temperature and composition as the input which reflects in terms of the final mass trapped in the engine during the closed part of the cycle. The total mixture mass determines the energy input to the cycle and hence the power delivered. Towards estimating the approximate peak load supported by the engine frame on PG, the manifold pressure is gradually increased while keeping the mixture temperature fixed. With an increase in the inlet charge pressure, while the load delivered increase, the post compression pressure and temperature will also increase leading to a reduction in the mixture auto-ignition time. As the manifold pressure is increased, up to a pressure of 1.85 bar corresponding to a load of 76 kWe, no end gas auto-ignition is observed. Beyond this, the model predicts end gas to auto-ignition as indicated in Figure 7, limiting the knock supported peak load to 76 kWe. The load of 76 kWe is very close to the estimated peak load of 74 kWe and delivered load of 72.8 kWe on the engine frame.

Analysis of the gas exchange process and quantifying various mean effective pressures

Ideally, under NA mode of operation, the transfer of energy between the piston and the working fluid during the gas exchange phase of the cycle (pumping work) is from the piston to the working fluid, signifying negative work and from the working fluid to the piston under TA mode of operation,[11] signifying positive work. The actual working conditions, however, differ significantly and an assessment of the work transfer during the gas exchange process is possible by the pressure–volume diagram. Figure 8 presents the pressure–volume diagram for the peak load under NA and TA mode of operation. Based on the pressure–crank angle and pressure–volume trace(s), the different mean effective pressure (MEP) values are consolidated in Table 6.

The scavenging section of the gas exchange process for the TA operation indicates a bi-modal profile, unlike the uni-modal profile for the NA mode. As the piston moves from the bottom dead centre (BDC) to the TDC, the pressure rises to a local maximum and progresses to reach a process minimum before attaining the maximum near the TDC. The bi-modal nature of the scavenging process for TA operation of the engine is mainly attributed to the higher mixture mass flow across the exhaust valve compared to NA operation. The pressure ratio across the exhaust valve will be significantly different as compared to NA mode of operation as the valve timing and movement profile remaining unchanged. The presence and response of different turbochargers for different quality and quantity of exhaust flow also affects the manifold pressure, in turn affecting the cylinder pressure.

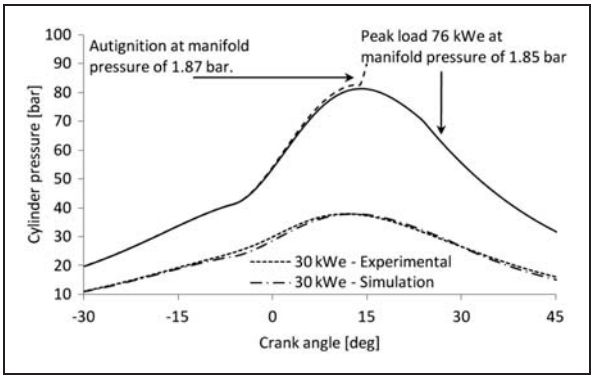

Figure 7. Knock limited peak load estimation from the zero-dimensional code.

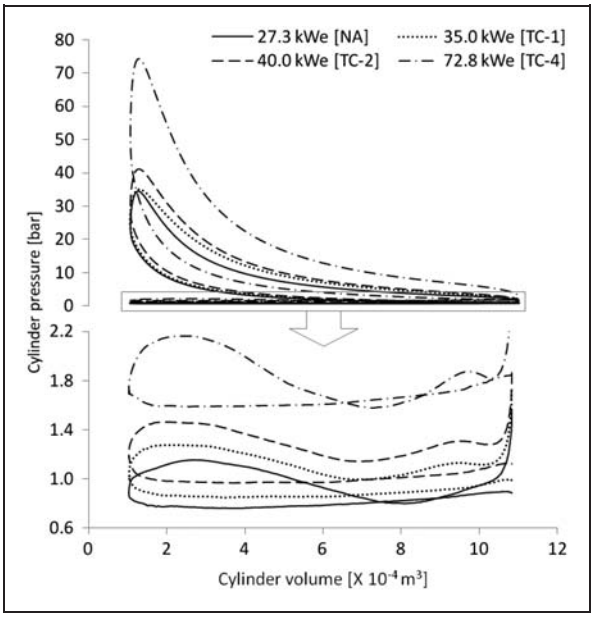

Figure 8. Peak load pressure volume diagram.
NA: naturally aspirated; TC: turbocharger.

It is interesting to note that, in case of NA mode of operation and at peak load TA operation at 72.8 kWe (TC–4), the scavenging cylinder pressure momentarily dips below the intake pressure. For this duration of the gas exchange process, the work transfer is positive and is reflected on the pumping MEP and the net indicated MEP. While Table 6 presents the absolute MEP numbers, towards comparing the performance in relation to the NA mode operation, the TA operation MEP values are normalized with the corresponding NA mode values and are presented in Figure 9. It can be observed that, for TC–1 and TC–2, in % terms, the increase in pumping MEP is much higher than the increase in the brake MEP as compared to NA mode operation. For TC–4, however, the brake MEP rise is significantly higher than the increase in the pumping MEP. The substantially higher rise in the brake MEP as compared to pumping MEP for TC–4 (attributed to the positive work contribution in the gas exchange process) as against the

Table 6. Peak load mean effective pressure values.

	NA mode	TC–1	TC–2	TC–4
BMEP (bar)	3.70	4.75	5.42	9.87
gIMEP (bar)	5.89	7.25	7.98	13.95
nIMEP (bar)	5.62	6.88	7.56	13.56
PMEP (bar)	0.27	0.37	0.42	0.39
FMEP (bar)	2.19	2.50	2.56	4.08

BMEP: brake mean effective pressure; gIMEP: gross indicated mean effective pressure; nIMEP: net indicated mean effective pressure; PMEP: pumping mean effective pressure; FMEP: frictional mean effective pressure.

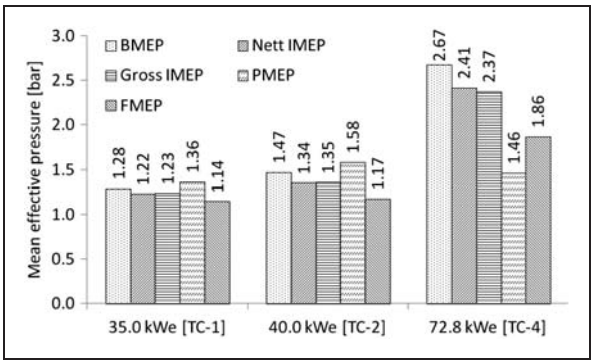

Figure 9. Normalized MEP values (TA to NA).
BMEP: brake mean effective pressure; IMEP: indicated mean effective pressure; FMEP: frictional mean effective pressure; PMEP: pumping mean effective pressure.

trend for TC–1 and TC–2 indicates the positive influence and hence the suitability of TC–4 for PG-fuelled operation.

Quantifying the pumping losses permits estimation of the rubbing losses in the engine. The total frictional loss of the engine (frictional MEP) is constituted of the pumping, accessories and the rubbing friction losses.[11] The power drawn by the accessories (radiator fan and starter battery charging) amount to about 0.81 bar MEP. Based on the accessories MEP and pumping MEP, the rubbing MEP for TC–1, TC–2 and TC–4 evaluates to 1.32, 1.33 and 2.88 bars, respectively. As can be observed, the rubbing friction component indicates an increasing trend constituting 53% of the frictional MEP at 35 kWe which increases to about 71% at 72.8 kWe load. The rather sharp increase in the rubbing MEP and correspondingly the frictional MEP at 72.8 kWe is attributed to the fact that the rubbing friction in the engine scales with the peak cylinder pressure.[11,42,43]

Comparison of turbocharger response

A general comparison of the performance of the three turbochargers is presented in this section. Figure 10 presents the variation of the pressure ratio with load

for the three turbochargers tested. The peak load pressure ratio and isentropic compression efficiency data is included inset. The pressure ratio and isentropic compression efficiency are both significantly low for TC–1 and TC–2.

The gas exchange process with the three turbochargers at a common load of 30 kWe (NA mode peak load without radiator) is presented in Figure 11. Comparing the gas exchange process at a fixed load primarily highlights the impact of the turbocharger while (significantly) discounting the factors associated with quality and quantity of the exhaust (which are not expected to differ significantly at the same load).

One of the first observations evident from Figure 11 is that, at the same load, the average scavenging process cylinder pressure increases from TC–1 to TC–2 to TC–4 making the impact of the turbine casing area and the upstream mass build up clear. The turbocharger TC–1, with a large turbine cross-sectional area of 10 cm^2 is over sized resulting in significant portion of the gases to move towards the exit without transferring energy to the impeller. This in turn causes the turbine and hence the compressor to spin slowly. Owing to the low impeller speed, due to the basic nature of centrifugal compressors,[33] the pressure ratio and the efficiency achieved are low. Replacing TC–1 with TC–2, a reduction in the turbine cross-sectional area from 10 cm^2 to 8 cm^2 and the compressor wheel diameter from 82 mm to 77 mm (TC–2), an improvement in the turbine inlet pressure is observed which reflects in terms of improved compressor pressure ratio and the load delivered by the engine. The improvement in the pressure ratio is, however, insufficient to deliver the required load. On switching from turbocharger TC–2 to TC–3, the turbine cross-sectional area reduces from 8 cm^2 to 6 cm^2. Engine operation with TC–3 caused significant turbine back pressure leading to both the turbine inlet pressure and temperature surpassing the safe operational limit and accordingly, further operation was suspended. Finally, the turbocharger TC–4 having 8 cm^2 turbine casing and 68 mm compressor wheel diameter is able to support higher pressure ratio and mass flow required to attain the designated load, indicating the suitability of TC–4. A detailed analysis of the turbocharger TC–4 is presented in the next section.

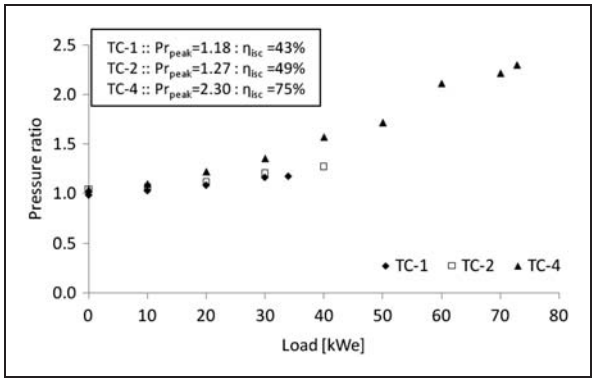

Figure 10. Pressure ratio and isentropic compression efficiency of the turbochargers.

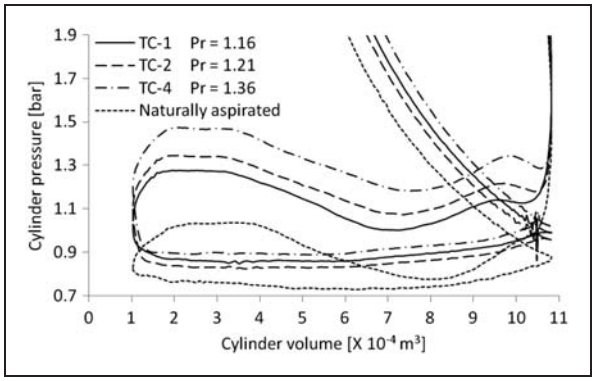

Figure 11. Gas exchange process for naturally aspirated (NA) and turbocharged after-cooled (TA) operation at 30 kWe load.

Performance analysis of turbocharger TC–4

Pressure and density ratio across the compressor. The purpose of a turbocharger compressor is to increase the mixture density by increasing the mixture pressure. However, mixture pressure rise is accompanied by an increase in the temperature, which partially offsets the increase in mixture density. To curtail the temperature rise, an after-cooler is introduced between the compressor outlet and the inlet manifold. Figure 12 shows the pressure and temperature ratio across the compressor and the compressor after-cooler assembly.

It can be observed that the introduction of the after-cooler while cooling the mixture to close to inlet conditions (as evident from the near flat trend

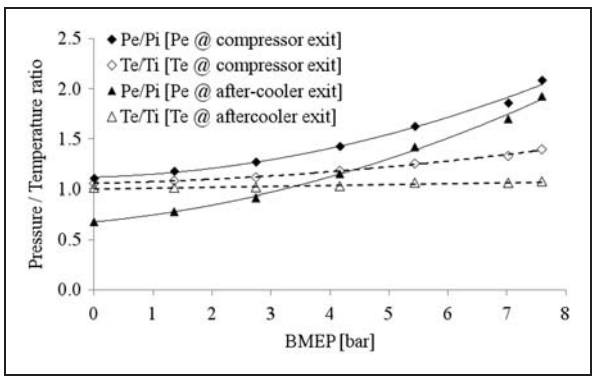

Figure 12. Pressure and temperature ratio across the compressor and the compressor-after cooler.
BMEP: brake mean effective pressure.

for the temperature ratio) also introduces some pressure drop due to the resistance to the flow. The useful pressure ratio is actually lower than unity due to this pressure drop till about 3.5 bar.

The combined effect of the compressor and after-cooler on the mass delivered to the engine over the entire load range can be appropriately gauged by considering the density ratio as presented in Figure 13. It can be observed that, despite the rise in temperature due to compression, the density ratio across the compressor remains higher than unity across the entire load range. Due to the pressure drop across the after-cooler, the density ratio is pushed below unity till about 3.5 bar brake MEP. It is also interesting to note that the density ratio across the compressor and after-cooler assembly surpasses the density ratio across the compressor only beyond 5.2 bar brake MEP. This implies that up to 5.2 bar brake MEP, amounting close to 50% of the load, the after-cooler is having a negative impact on the density and hence the mass delivered.

With the density ratio across the compressor being higher than unity over the entire load range and the after-cooler actually having a negative influence up to about 50% of the load, the possibility of bypassing the after-cooler is explored. In bypassing the after-cooler, one of the primary concerns pertains to end mixture auto-ignition in the absence of cooling of the mixture. To address this issue, the impact of mixture inlet temperature on engine knock is addressed. Without actually bypassing the after-cooler, the mixture temperature is controlled by controlling the cooling water flow rate through the after-cooler and the cylinder pressure traces are monitored to identify knock, if any.

The nature of combustion in the cylinder in terms of the absolute cylinder pressure trace and the low frequency filtered pressure trace, at peak load of 72.8 kWe at different mixture inlet temperatures is shown in Figure 14. At the peak load, the compressor pressure ratio is 2.30 while compressor exit temperature is 140°C. The mixture temperature at peak load under normal operating conditions is at 53 ± 1°C and as the water flow rate through the after-cooler is reduced, up to about 55°C, the combustion remains normal as indicated in Figure 14(a). As the water flow rate is further reduced, beyond 55°C up to about 58°C, some small disturbances occurring only intermittently are evident on the pressure trace as indicated in Figure 14(b). The initiation of end gas auto-ignition is evident at this stage. Between 58°C and 65°C, well-established knock can be observed as indicated in Figure 14(c) and the frequency of occurring is more than 50% in a acquisition of 250 consecutive cycles. At mixture temperatures beyond 65°C, heavy knocking is observed as indicated in Figure 14(d). At this state, the distinct ringing noise indicative of heavy knock is also audible. Considering that beyond 55°C trace knock is evident, while the mixture temperature is already at 53 ± 1°C at the compressor exit at a load of 10 kWe, the use of un-cooled mixture is ruled out and the after-cooler becomes an indispensable component under TA operation.

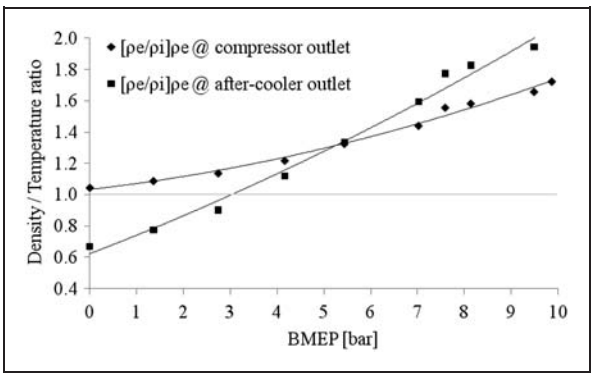

Figure 13. Density ratio across the compressor and after cooler.
BMEP: brake mean effective pressure.

The zero-dimensional model is used to identify the knock limited mixture temperature at various loads as indicated in Figure 15. The predicted temperatures are between 2° and 4° lower than the actual temperatures at which knock is observed. In the absence of exact replication of the prevailing engine conditions, which is a fundamental limitation of any model and specifically so for a zero-dimensional mode, the deviations in the predicated results are along expected lines. However, the approximate range in which the knock is initiated in the engine is successfully indicated by the zero-dimensional models.

Thermodynamic analysis of the turbocharger. Thermodynamic analysis of the turbocharger permits the estimation of the turbine and compressor isentropic efficiency and turbocharger mechanical efficiency. The variation of the actual compressor inlet and exit temperature, the isentropic exit temperature and the isentropic efficiency with load is shown in Figure 16. The maximum isentropic efficiency is 74.5% and is in line with literature reported values of around 75%[11,10] and the identified efficiency on the compressor map (refer Figure 2). Dasappa et al.[10] have reported an isentropic efficiency of around 77% for a different engine turbocharger at a load of 110 kWe operating on PG. The actual peak load compressor work is 14 kWe which amounts to 20% of the peak load delivered by the engine.

Figure 17 presents the variation of the measured inlet and exit temperatures along with the isentropic and corrected exit temperatures for the turbine. The corrected exit temperature is estimated by accounting

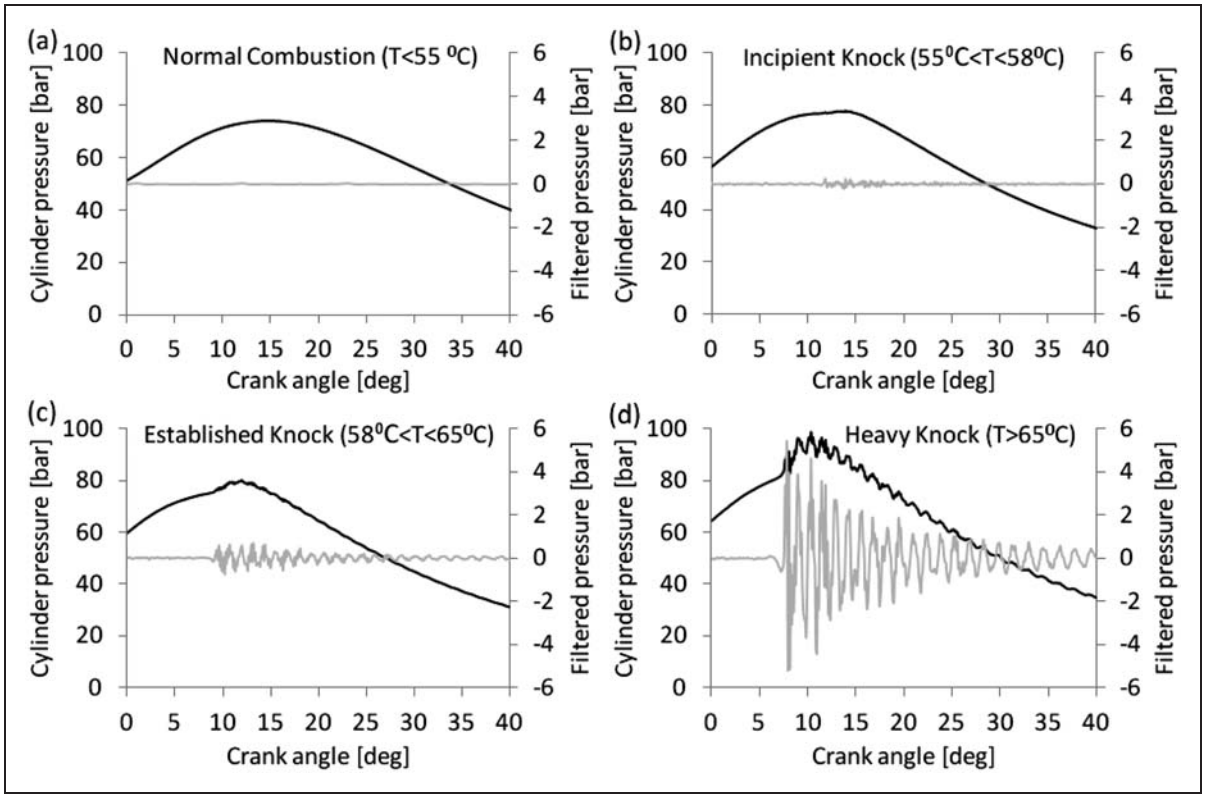

Figure 14. Nature of combustion at various mixture inlet temperatures.

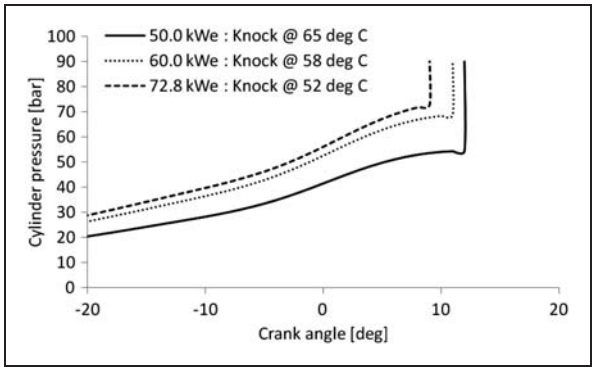

Figure 15. Knock limited manifold temperature prediction at different loads.

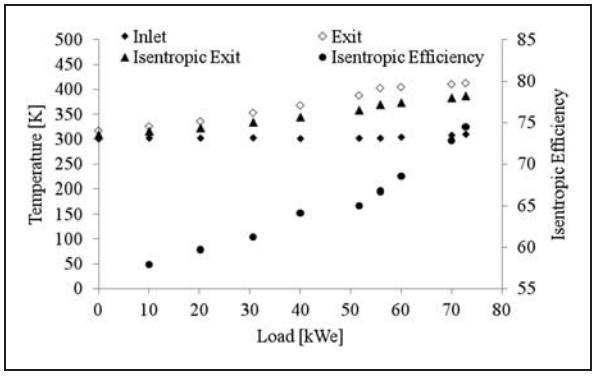

Figure 16. Compressor actual and isentropic temperatures and isentropic efficiency.

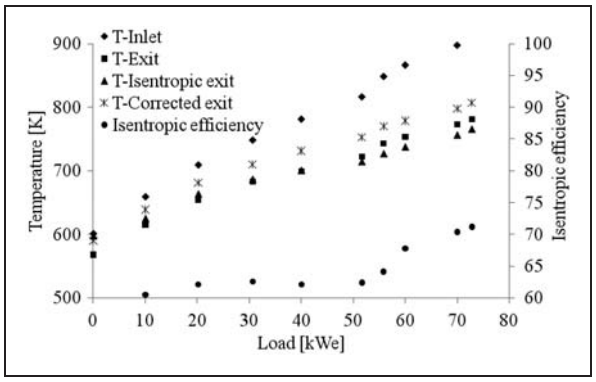

Figure 17. Turbine temperatures and isentropic efficiency.

for the heat losses from the turbine. The isentropic turbine efficiency approaches close to 73% at the peak load while it is between 60% and 65% at the other loads. It is important to note that the turbine efficiency remains rather flat at around 63% till about 50 kWe and then increases with load.

Turbocharger mechanical efficiency. Figure 18 shows the variation of turbocharger mechanical efficiency, the ratio of compressor to turbine power, with load. The peak load turbine work at 17.4 kW amounts to about 5% of the input energy and 24% of the engine output. The heat transfer losses from the turbine casing, based on surface area and temperature measurements, constitute close to 20% of the turbine

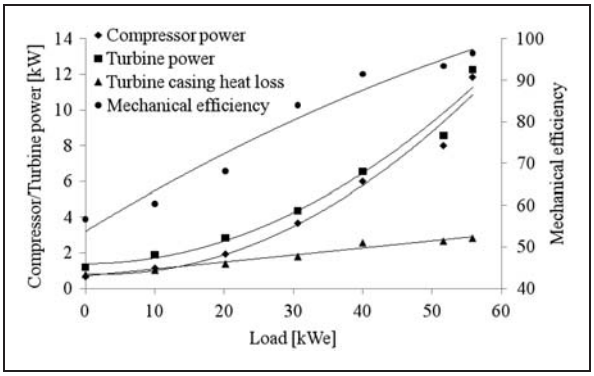

Figure 18. Energy transfer components and mechanical efficiency for TC–4.

work. The mechanical efficiency varies from under 60% at no load conditions to reach a peak of about 88%.

Compressor map performance mapping. Figure 19 presents the TC–4 compressor map with the predicted and actual performances mapped. At higher loads, the actual corrected mass flow rate is higher than the estimated value (5% at peak load). This is attributed to the drop in the inlet line pressure from 0.95 ± 0.02 bar to 0.88 bar as the load increases from 55.0 kWe to full load. The peak load operating efficiency of the compressor at 73% is close to the calculated isentropic efficiency of 74.5%.

Summary of 6B5.9 engine performance

Having identified the turbocharger to deliver the target load, a comparison of some critical parameters pertaining to the engine operation under naturally aspirated and turbocharged mode covering the native turbocharger and the optimized turbocharger is consolidated in Table 7.

The increase in the brake MEP with the optimized turbocharger from the NA mode is 167% which is substantial. With the same engine block delivering more than double the power, profound economic benefits apart from the efficiency improvements are obvious. With near complete recovery of the identified recovery potential, the specific biomass consumption indicates a reduction of over 26% and 17% giving an overall (biomass to electricity) efficiency of 24% with the engine efficiency at 32%. The engine power density (power per unit swept volume) with the optimized turbocharger at 12.34 kWe/l is comparable with conventional fuelled engines and dedicated PG engine (GE Jenbacher – JGS 320 GS with power density of 12.1 kWe/l for PG-fuelled operation[44]).

Emissions on 6B5.9 under both NA and TA mode PG-fuelled operation have also been captured under wide open throttle conditions. The emissions are compared with standards adopted by Central Pollution Control Board (CPCB), India and the Environmental Protection Agency (EPA), USA as in Table 8. Reporting and comparing emissions remains a challenge considering the fact that different countries adopt different standards and units of reporting emissions and the current standards available all deal with gasoline/diesel fuel with some latest standards including NG. At the time of this reporting, there are no established standards for emissions from renewable fuels and almost all standards recommend adopting NG limits for gaseous renewable fuels. For an exhaust system without a catalytic converter, the CO and NOx emissions under TA mode are well within the prescribed limits of both Indian and US standards.

Table 7. Response of 6B5.9 under PG-fuelled NA and TA mode of operation.

	Naturally aspirated	Turbo unoptimized	Turbo optimized
BMEP (bar)	3.70	4.75	9.87
SBC (kg/kWh)	1.35	1.2	1.0
Overall efficiency (%)	18	20	24
Specific weight (kg/kWe)	38.4	30.0	14.4
Load per volume (kWe/l)	4.64	5.93	12.34

NA: naturally aspirated; TA: turbocharged after-cooled; BMEP: brake mean effective pressure; SBC: specific biomass consumption.

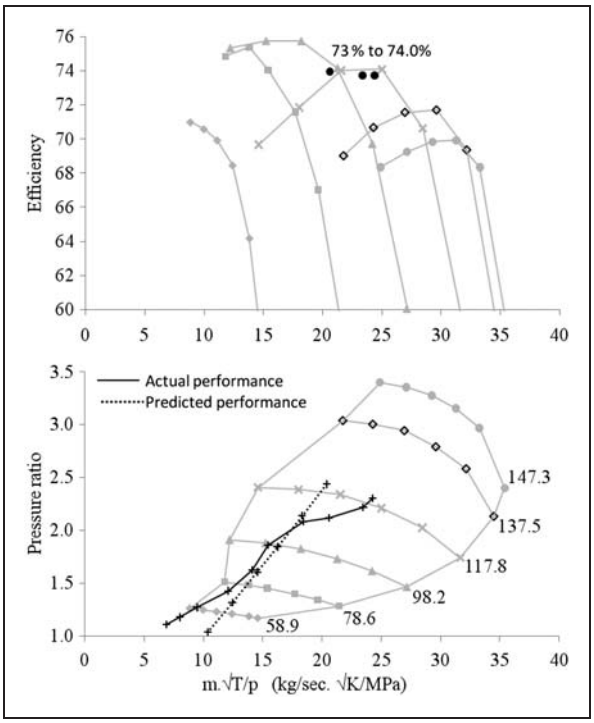

Figure 19. Predicted and actual performance mapping on HX30W compressor map.

Table 8. Emissions from 6B5.9 under NA and TA mode of operation.

Description	Mode	O_2%	Units	CO	NO_x	HC
6B measured	NA	5	mg/nm^3	2994.52	132.81	6.56
			g/kWh	11.66	0.52	0.03
		15	mg/nm^3	1156.26	51.27	2.51
			g/kWh	4.50	0.20	0.01
	TA	5	mg/nm^3	2403.01	640.12	0.00
			g/kWh	8.74	2.33	0.00
		15	mg/nm^3	931.45	248.11	0.00
			g/kWh	3.39	0.90	0.00
CPCB (India)[a]		15	g/kWh	623	16.1 (NOx + HC)	
CPCB (India)[b]				3.5	9.2	1.3
EPA (USA)[c]				6.5	3.8 (NOx + HC)	

NA: naturally aspirated; TA: turbocharged after-cooled.
[a]Refers to generators run on gasoline/kerosene up to 19 kW.
[b]Refers to generators run on diesel up to 800 kW.
[c]Refers to non emergency SI natural gas engines in the 19–75 kW rating.

Conclusions

The importance of turbocharger matching on adoption of conventional fuel engines for operation with low energy content gas has been addressed. Assessment of PG-fuelled operation of three diesel engines of different power rating, converted for SI operation, indicates power de-rating in excess of 50%, with around 75% of the total de-rating attributed to the turbocharger mismatch. The approximate knock limited peak load is also identified from a zero-dimensional code tuned for PG-fuelled operation. The recovery potential is realized by turbocharger optimization on 6B5.9, a six-cylinder, 5.9 l engine.

The engine, on fuelling with PG in SI mode, delivers a peak load of 27.3 kWe and 36 kWe under naturally aspirated and turbocharged mode, respectively, representing a de-rating of 70% and 60% over the corresponding diesel rating. Breakup of the de-rating has indicated a contribution of 18%, 9% and 35% (of diesel rating) due to CR reduction, lower mixture calorific value and turbocharger mismatch, respectively. The recovery potential from naturally aspirated conditions is established at 39 kWe to deliver a peak load of 74 kWe while the zero-dimensional code indicates a knock limited peak load of 76 kWe. A change in the mixture flow rate from about 250 kg/h to 520 kg/h is required to support the higher load. The engine with the optimized turbocharger supports a knock limited peak load of 72.8 kWe at a compressor pressure ratio of 2.30 representing 98.4% of the target load. The thermodynamic analysis of the compressor and the turbine indicate an isentropic efficiency of 74.5% and 73%, respectively. On the performance of the 6B5.9 engine, the specific biomass consumption reduces from 1.2 kg/kWh to 1.0 kg/kWh with engine efficiency at 32% and the biomass to electricity efficiency at 24%. The engine power density of 12.34 kWe/l is comparable with conventional fuelled engines.

The current work has identified turbocharger mismatch as one of the principal contributing factors of engine de-rating in the operation of engines designed for conventional fuels with alternative fuels. The possibility of recovery of non-thermodynamic de-rating and improving the engine power density by turbocharger selection and optimization has been established. The validity of using a tuned zero-dimensional code for approximating the peak supported load is also established. The methodology of turbocharger selection and optimization towards operation of an engine designed for conventional fuels with PG has been brought out. It is assessed that the principle can in general, be extended to other engine capacities for operation with fuels other than the designated fuel with the iteration required for optimization depending on the extent of difference between the base fuel and the alternative fuel.

Acknowledgement

The authors thank all the team members from Cummins India Limited who participated in the investigation.

Funding

The work was supported by the Ministry of New and Renewable Energy, Government of India, New Delhi.

References

1. Demirbas A. Progress and recent trends in biofuels. *Prog Energy Combust Sci* 2007; 33: 1–18.
2. Jiménez-Rodríguez R and Sánchez M. Oil price shocks and real GDP growth: empirical evidence for some OECD countries. *Appl Econ* 2005; 37: 201–228.

3. Birol F and Argiri M. World energy prospects to 2020. *Energy* 1999; 24: 905–918.
4. Krewitt W, Simon S, Graus W, et al. The 2°C scenario – a sustainable world energy perspective. *Energy Policy* 2007; 35: 4969–4980.
5. Wyman CE. Alternative fuels from biomass and their impact on carbon dioxide accumulation. *Appl Biochem Biotechnol* 1994; 45: 897–915.
6. Demirbas A. Current advances in alternative motor fuels. *Energy Exploration Exploitation* 2003; 21: 475–487.
7. Balat M. Current alternative engine fuels. *Energy Sources* 2005; 27: 569–577.
8. Astbury GR. A review of the properties and hazards of some alternative fuels. *Process Saf Environ Protect* 2008; 86: 397–414.
9. Dasappa S, Sridhar G and Paul PJ. Adaptation of small capacity natural gas engine for producer gas operation. *Proc IMechE, Part C: J Mechanical Engineering Science* 2011; 226: 1568–1578.
10. Dasappa S, Sridhar HV and Muzumdar I. Experiments on and thermodynamic analysis of a turbocharged engine with producer gas as fuel. *Proc IMechE, Part C: J Mechanical Engineering Science* 2012; 226: 1004–1015.
11. Heywood JB. *Internal combustion engine fundamentals*. USA: McGraw-Hill Education, 1988.
12. Battistoni M, Grimaldi CN and Mariani F. Numerical study of SI engine part load operating conditions using different VVA strategies. *ASME Conf Proc* 2011; 2011: 943–953.
13. Bridgwater AV, Toft AJ and Brammer JG. A techno-economic comparison of power production by biomass fast pyrolysis with gasification and combustion. *Renew Sust Energy Rev* 2002; 6: 181–246.
14. Siemons RV. Identifying a role for biomass gasification in rural electrification in developing countries: the economic perspective. *Biomass Bioenergy* 2001; 20: 271–285.
15. Diakoulaki D and Karangelis F. Multi-criteria decision analysis and cost-benefit analysis of alternative scenarios for the power generation sector in Greece. *Renew Sust Energy Rev* 2007; 11: 716–727.
16. Dasappa S. On the estimation of power from a diesel engine converted for gas operation: a simple analysis. In: *Proceedings of the seventeenth national conference on I.C. engines and combustion*, 2001, pp.167–174.
17. Dasappa S, Paul PJ, Mukunda HS, et al. Biomass gasification technology – a route to meet energy needs. *Curr Sci* 2004; 87: 908–916.
18. Mukunda HS. *Understanding combustion*. Hyderabad, India: Universities Press (India) Private Limited Publication, 1989.
19. Quaak P, Knoef H and Stassen HE. *Energy from biomass: a review of combustion and gasification technologies*. vol 23, Washington DC, USA: World Bank Publications, 1999.
20. Reed RJ. *Combustion handbook*. Cleveland, OH: North American Mfg. Co, 1986.
21. Yu G, Law CK and Wu CK. Laminar flame speeds of hydrocarbon+air mixtures with hydrogen addition. *Combust Flame* 1986; 63: 339–347.
22. Sridhar G. *Experimental and modeling studies of producer gas based spark-ignited reciprocating engines*. PhD Thesis, Department of Aerospace, Indian Institute of Science, 2003.
23. Dasappa S and Shivapuji AM. Experimental studies on multi-cylinder natural gas engine fueled with producer gas. In: *Proceedings of the 19th European biomass conference and exhibition*, 2011, pp.974–980.
24. Ghojel JI. Review of the development and applications of the Wiebe function: a tribute to the contribution of Ivan Wiebe to engine research. *Int J Engine Res* 2010; 11: 297–312.
25. Sridhar G, Paul PJ and Mukunda HS. Biomass derived producer gas as a reciprocating engine fuel – an experimental analysis. *Biomass Bioenergy* 2001; 21: 61–72.
26. Sridhar G, Sridhar HV, Dasappa S, et al. Development of producer gas engines. *Proc IMechE, Part D: J Automobile Engineering* 2005; 219: 423–438.
27. Shashikantha PPP. Spark ignition producer gas engine and dedicated compressed natural gas engine – technology development and experimental performance optimization. SAE paper 1999-01-3515, 1999.
28. Watson N and Janota MS. *Turbocharging the internal combustion engine*. Hampshire, UK: MacMillan, 1982.
29. Shivapuji AM and Dasappa S. Experiments and zero D modeling studies using specific Wiebe coefficients for producer gas as fuel in spark-ignited engines. *Proc IMechE, Part C: J Mechanical Engineering Science* 2013; 227: 504–519.
30. Shivapuji AM and Dasappa S. Knock and its prediction in producer gas fuelled SI engines. In: *Proceedings of the international conference on polygeneration strategies*, Vienna, Austria, 2013, pp.227–236.
31. Colin RF and Allan TK. *Internal combustion engines: applied thermo sciences*. New York, USA: John Wiley & Sons, Inc, 2001.
32. Lumsden G, OudeNijeweme D, Fraser N, et al. Development of a turbocharged direct injection downsizing demonstrator engine. *SAE Int J Engines* 2009; 2: 1420–1432.
33. Cohen H, Rodgers GFC and Saravanamuttoo HIH. *Gas turbine theory*. New Delhi, India: Pearson Education, 1987.
34. Cummins Diesel Generator Set – Specification Sheet – VTA28, http://cumminspower.com/www/common/templatehtml/technicaldocument/SpecSheets/Diesel/emea/SS_VTA28.pdf (2012, accessed 2 November 2012).
35. Cummins Diesel Generator Set – Specification Sheet – NTA855, http://www.cumminspower.com/www/common/templatehtml/technicaldocument/SpecSheets/Diesel/na/s-1581.pdf (2012, accessed 2 November 2012).
36. Cummins Diesel Generator Set – Specification Sheet – 6BT5.9, http://www.cumminspower.com/www/common/templatehtml/technicaldocument/SpecSheets/Diesel/na/s-1576.pdf (2012, accessed 2 November 2012).
37. Pipitone E and Beccari A. A study on the use of combustion phase indicators for MBT spark timing on a bi-fuel engine. SAE paper 2007-24-0051, 2007.
38. Hubbard M, Dobson PD and Powell JD. Closed loop control of spark advance using a cylinder pressure sensor. *J Dyn Syst Meas Control* 1976; 98: 414.
39. Lazarescu D, Lazarescu V and Ungureanu M. Knock detection based on SOM. In: *NEUREL 2004 – 7th*

seminar on neural network applications in electrical engineering, 2004, pp.117–120. Serbia and Montenegro: University of Belgrade.
40. Hudson C, Gao X and Stone R. Knock measurement for fuel evaluation in spark ignition engines. *Fuel* 2001; 80: 395–407.
41. Stanković L and Böhme JF. Time–frequency analysis of multiple resonances in combustion engine signals. *Signal Process* 1999; 79: 15–28.
42. Hoshi M and Baba Y. A study of piston friction force in an internal combustion engine. *ASLE Trans* 1986; 30: 444–451.
43. Nakada M. Trends in engine technology and tribology. *Tribol Int* 1994; 27: 3–8.
44. Ge Jenbacher – Technical Description – JGS 320, http://www.energyregulator.tas.gov.au/domino/otter.nsf/LookupFiles/AGL_Hobart_Technical_Description.pdf (2012, accessed 2 November 2012).
45. Cummins Natural Gas Generating Set – Specification Sheet – GTA1070, http://www.planbfirst.com/May 2009 Updates/SpecSheet/Gas 380spec.pdf (2012, accessed 2 November 2012).
46. Cummins Natural Gas Generating Set – Specification Sheet – GTA855, http://cumminsengines.com/assets/pdf/og_gc_g855_gta855.pdf (2012, accessed 2 November 2012).

Appendix 1

Notation

a	Wiebe efficiency factor
BDC	bottom dead centre
CI	compression ignition
CIL	Cummins India Limited
CR	compression ratio
CTT	cumming turbo technologies
FET	filling and emptying technique
IC	internal combustion
LCV	low calorific value
m	Wiebe shape factor
MBT	maximum brake torque
MEP	mean effective pressure
NG	natural gas
PG	producer gas
SFC	specific fuel consumption
SI	spark ignited
TA	turbocharged after-cooled
TDC	top dead centre

Appendix 2. Engines performance

Table 9. Performance of 500 kWe engine (*E* – 500) with different fuels.

Fuel	Diesel[34]	Natural gas[45]	Producer gas[10]
Cylinders/total displacement (l)	12 (twin bank)/28		
Compression ratio	13.1:1	10:1	
Turbocharger	Holset LGK series		
Specified/recorded engine performance			
Peak load (kWe)	500	355	240
Compressor pressure ratio	2.4	1.5	1.5
BMEP (bar)	14.3	10.1	6.9
Power density (kWe/l)	17.9	12.7	8.6
SEC (MJ/kWh)	9.1	10.0	13.0
Mixture LCV (MJ/kg)	2.3	2.6	2.1
Assessment of engine de-rating due to fuel change			
BMEP de-rating over diesel (%)	–	29.4	51.7
BMEP de-rating over NG (%)	–	–	31.7
De-rating due to CR reduction	–	$3.1 \times 3 = 9.3\%$ or 46.5 kW	
De-rating due to mix LCV (ref diesel)	–	–	43.5 kW
De-rating due to mix LCV (ref NG)	–	–	68.3 kW

Table 10. Performance of 250 kWe engine (*E* – 250) with different fuels.

Fuel	Diesel[35]	Natural gas[46]	Producer gas[10]
Cylinders/total displacement (l)	6 (single bank)/14		
Compression ratio	14.0:1	8.5:1	
Turbocharger	Holset LGK series		
Specified/recorded engine performance			
Peak load (kWe)	250	168	120
Compressor pressure ratio	2.4	1.5	1.5
BMEP (bar)	14.3	9.6	6.9
Power density (kWe/l)	17.9	12.0	8.6
SEC (MJ/kWh)	9.1	10.0	13.0
Mixture LCV (MJ/kg)	2.3	2.6	2.1
Assessment of engine de-rating due to fuel change			
BMEP de-rating over diesel (%)	–	32.9	51.7
BMEP de-rating over NG (%)	–	–	28.1
De-rating due to CR reduction	–	$5.5 \times 3 = 16.5\%$ or 41.3 kW	
De-rating due to mix LCV (ref diesel)	–	–	21.7 kW
De-rating due to mix LCV (ref NG)	–	–	32.3 kW

Table 11. Performance of 90 kWe engine (*E* – 90) with different fuels.

Fuel	Diesel[36]	Natural gas[9]	Producer gas[9]
Cylinders/total displacement (l)	6 (single bank)/5.9		
Compression ratio	16.5:1	10.5:1	
Turbocharger	Holset HX series		
Specified/recorded engine performance			
Peak load (kWe)	90	70	36
Compressor pressure ratio	2.2	1.5	1.2
BMEP (bar)	12.2	9.5	4.9
Power density (kWe/l)	15.3	11.9	6.1
SEC (MJ/kWh)	9.1	10.0	13.0
Mixture LCV (MJ/kg)	2.3	2.6	2.1
Assessment of engine de-rating due to fuel change			
BMEP de-rating over diesel (%)	–	22.1	59.8
BMEP de-rating over NG (%)	–	–	48.4
De-rating due to CR reduction	–	$6 \times 3 = 18\%$ or 16.2 kW	
De-rating due to LCV (ref diesel)	–	–	7.8 kW
De-rating due to LCV (ref NG)	–	–	13.5 kW